Neuronal Death and Perinatal Lethality in Voltage-Gated Sodium Channel α_{II}-Deficient Mice

R. Planells-Cases,* M. Caprini,* J. Zhang,* E. M. Rockenstein,[†] R. R. Rivera,* C. Murre,* E. Masliah,[†] and M. Montal*

Departments of Biology* and Neurosciences,[†] University of California San Diego, La Jolla, California

ABSTRACT   Neural activity is crucial for cell survival and fine patterning of neuronal connectivity during neurodevelopment. To investigate the role in vivo of sodium channels (NaCh) in these processes, we generated knockout mice deficient in brain NaChα_{II}. NaCh$\alpha_{II}^{-/-}$ mice were morphologically and organogenically indistinguishable from their NaCh$\alpha^{+/-}$ littermates. Notwithstanding, NaCh$\alpha_{II}^{-/-}$ mice died perinatally with severe hypoxia and massive neuronal apoptosis, notably in the brainstem. Sodium channel currents recorded from cultured neurons of NaCh$\alpha_{II}^{-/-}$ mice were sharply attenuated. Death appears to arise from severe hypoxia consequent to the brainstem deficiency of NaChα_{II}. NaChα_{II} expression is, therefore, redundant for embryonic development but essential for postnatal survival.

INTRODUCTION

A long-held tenet considers that electrical activity is a crucial component in brain development and synaptogenesis (Katz and Shatz, 1996; Catalano and Shatz, 1998; Ikonomidou et al., 1999). Action potentials propagated along the axon evoke the release of neurotransmitters at the synaptic terminal and thereby trigger neuronal signaling. Voltage-gated sodium channels (NaChs) are responsible for the inward flow of sodium current across the neuronal membrane during the rising phase of an action potential (Armstrong and Hille, 1998). NaChs are heteromeric membrane proteins that consist of one α subunit that determines the permeation and gating properties of the channel, and two different β subunits that modulate channel kinetics and density (Catterall, 1995; Hartshorne et al., 1985). Four different α subunit genes encoding tetrodotoxin-sensitive NaChs have been identified in mammalian neurons: α_I, α_{II}, α_{III}, and α_{VIII}, also denoted *SCN1A, SCN2A, SCN3A, SCN8A,* in keeping with the systematic mammalian gene symbols (cf. Plummer and Meissler, 1999). NaChα_{II} is the most abundant in rostral regions of the central nervous system (CNS) (cortex, hippocampus, striatum, and midbrain) (Beckh et al., 1989; Felts et al., 1997; Ahmed et al., 1992; Schaller et al., 1995; Smith et al., 1998). The molecular heterogeneity of NaCh α subtypes implies functional differences. Indeed, the mouse NaCh *SCN8A* and its rat ortholog NaCh6 are abundant in the cerebellum, and *SCN8A*

determines a persistent sodium conductance that plays a key role in the firing properties of Purkinje neurons (Schaller et al., 1995; Smith et al., 1998). And a loss-of-function point mutation of *SCN1B*, the gene encoding a NaCh β1 subunit, was identified in human generalized epilepsy with febrile seizures (Wallace et al., 1998). In addition, neural activity serves a crucial role during the development of the brain in the control of neuronal survival (Ikonomidou et al., 1999) and in synaptogenesis (Katz and Shatz, 1996; Catalano and Shatz, 1998). It is well recognized, especially in the visual system, that blockade of NaChs by tetrodotoxin alters drastically the fine patterning of neuronal connectivity (Katz and Shatz, 1996; Catalano and Shatz, 1998). And blockade of glutamate stimulation through NMDA receptors in the developing brain results in massive apoptotic neurodegeneration (Ikonomidou et al., 1999). To investigate the role in vivo of NaChs in neuronal apoptosis and synaptogenesis, and to develop an animal model to identify the function of specific NaChs, we used gene targeting (Capecchi, 1989) to generate knockout mice deficient in the brain sodium channel α_{II} subunit (NaChα_{II} or *SCN2A*). Mice homozygous for the mutation (NaCh$\alpha_{II}^{-/-}$) die perinatally with severe hypoxia and extensive neuronal cell death, presumably resulting from the brainstem deficiency of the NaChα_{II} gene product. A preliminary account of this research was presented elsewhere (Planells-Cases et al., 1999).

MATERIALS AND METHODS

Generation of NaChα_{II}-deficient mice

All procedures involving mice conformed with institutional and National Institutes of Health guidelines. The targeting vector, *Naneo*, contains ~9.5 kb of mouse genomic DNA encompassing exon 1 of NaChα_{II}, which was interrupted with the *neo*[r] gene (Fig. 1 *A*). Homologous recombination between the target locus and the targeting construct leads to a modified gene that now contains the positively selectable gene and truncates the NaChα_{II} protein after the seventh amino acid. To construct *Naneo*, 2×10^5 λ bacteriophages containing genomic DNA from an OLA129 mouse strain library were screened using a human brain NaChα_{II} cDNA probe, (nt −248
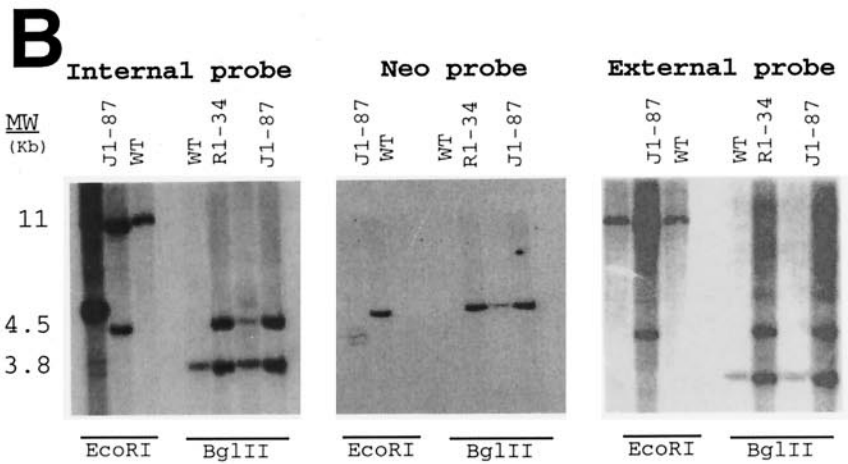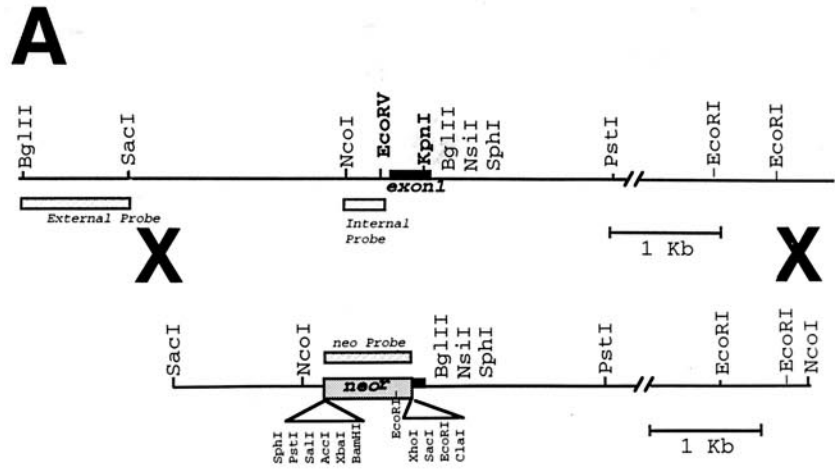
FIGURE 1 Targeted disruption of the NaChα_{II} locus. (*A*) Recombination design between the chromosomal locus (*top*) and the targeting vector *Naneo* (*bottom*). The *Neo*[r] gene replaced most of exon 1. The replaced fragment was 700 nt larger than the excised exon 1. Internal, external, and neo probes are indicated as shaded rectangles; scale bars are shown under each clone. (*B*) Southern blot analysis of wild-type, J1–87, and R1–34 ES cell clones digested with *Eco*RI and *Bgl*II. The same blot was sequentially hybridized with internal, external, and neo probes. (*C*) PCR analysis of genomic DNA from NaCh$\alpha_{II}^{+/+}$, NaCh$\alpha^{+/-}$, and NaCh$\alpha_{II}^{-/-}$ littermates. The 0.45-kb band corresponds to the wild-type allele, and the 1.3-kb band indicates a NaChα_{II} null allele. (*D*) Southern blot analysis of the same tail genomic DNA digested with *Bgl*II and labeled with internal probe.
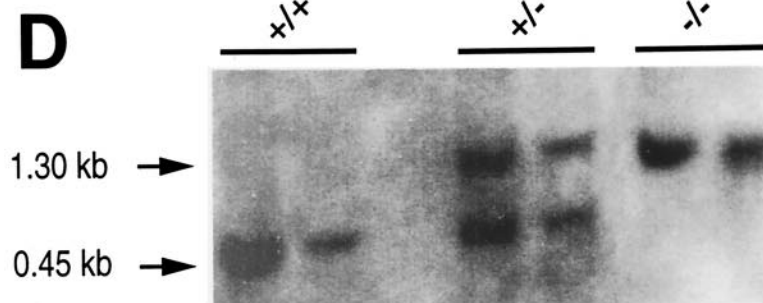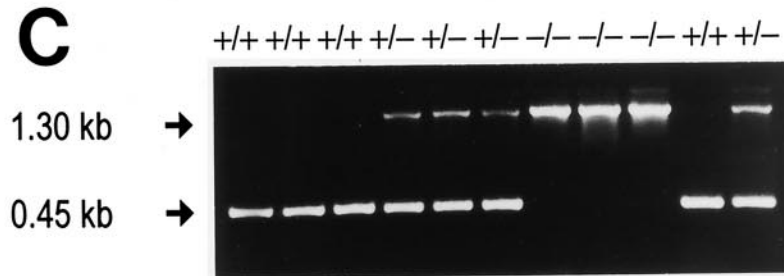
to 605 in the cDNA sequence) (Ahmed et al., 1992). Two clones were isolated; restriction analysis, in combination with Southern blot and sequencing, identified two overlapping inserts, both containing the entire exon 1 of the $NaCh\alpha_{II}$ gene. Na164/pGEM5Z was constructed in two steps. An 8-kb *Nco*I fragment, isolated from bacteriophage clone 2, was subcloned in pGEM5Z (Promega) and named *Na16*. In addition to exon 1, *Na16* contained ~7.5 kb of homologous flanking intron sequence in the 5′ end and ~500 nt at the 3′ end. No other exons were identified by Southern blot analysis using as probes different cDNA fragments. To increase the extent of homology at the 3′ end, an additional fragment of 2.4 kb, *Na64*, was subcloned at the *Eco*RV site of *Na16* to generate *Na164*. Overlapping sequences between the 8- and 2.4-kb fragments were sequenced and confirmed. The clone *Na164* was the basis for the targeting construct. A 325-nt *Kpn*I-*Eco*RV fragment that contains all except the first seven amino acids of exon 1 was excised from *Na164* and replaced by an *Eco*RV-*Hin*dIII insert containing the neo^r gene from pHA178 (a gift from Hein TeRiele). To identify targeting events, three different probes were designed (Fig. 1): the internal probe, a ~500-nt *Nco*I-*Eco*RV fragment flanking exon 1 in the 3′ end; the external probe, a ~1-kb *Bgl*II-*Sac*I fragment that is adjacent but not contained in the targeting construct; and a probe generated from the neo^r gene. J1 and R1 ES cells were transfected with *Naneo* after linearization with *Apa*I, thus generating ~7.5 kb of homology in the 5′ UTR, followed by seven amino acids of exon 1, and ~1.9 kb of homology in the 3′ UTR, surrounding neo^r (Fig. 1 *A*). Electroporated cells were subjected to positive-negative selection for 8 days in 150 μg/ml G418 (GIBCO-BRL). Positive colonies were expanded and analyzed by Southern blot. Thereafter, genomic DNA was isolated, analyzed by digestion with *Bgl*II and *Eco*RI, separately, and sequentially labeled with the internal, external, and neo^r probes (Fig. 1 *B*). Two targeted ES cell clones, R1–34 and J1–87, were injected into C57BL/6 mouse blastocysts. About six to eight blastocysts were implanted per pseudopregnant female. From J1–87 implants, no chimeric males were born and the single >90% chimeric female was sterile. From R1–34 implants, one wild-type female, two ≤30% chimeric females, and four >90% chimeric males were born. Chimeric males were mated with C57BL/6J females to set up a breeding colony and test for germline transmission of the mutant allele. Heterozygous F1 animals have been intercrossed through more than five generations. Genotyping of tail DNA with polymerase chain reaction (PCR) required two primers flanking the neo^r gene insertion. The sense primer was (5′TGCGAGGAGCTAAACAGTGATTAAAG3′), and the antisense primer was (5′GGCTCCATTCCCTTATCAGACCTACCC3′).

RNase protection assay

Levels of specific mRNAs were determined using solution hybridization RNase protection assays (RPAs) (Rockenstein et al., 1995). Poly A+ RNA was extracted from adult mouse brain, and reverse transcriptase-polymerase chain reaction (RT-PCR) was used to generate a 239-nt murine $NaCh\alpha_{II}$ riboprobe with primers derived from the rodent sequence (GenBank accession number M22254, nt 4965–5204). The actin riboprobe was nt 480–559 (GenBank accession number X03672). Amplification products were subcloned into pCRII (Invitrogen), and T7 or SP6 RNA polymerase was used to generate ^{32}P-labeled antisense riboprobes from 100 ng of linearized plasmids. Total RNA was isolated from snap-frozen tissues with the TRI reagent and stored in Formazol buffer (Molecular Research Center) at −20°C. Statistical analysis of differences between the three groups of mice was performed utilizing the one-factor analysis of variance test.

Western blot analysis

Brains were homogenized, fractionated into cytosolic and particulate components, and subjected to sodium dodecyl sulfate-polyacrylamide gel electrophoresis (SDS-PAGE) on 7% gels (Masliah et al., 1998b). Gels were blotted onto nitrocellulose membranes, and blots were incubated overnight with subunit-specific antipeptide antibodies (Alomone) (Westenbroek et al., 1992) (0.16 μg/ml $NaCh\alpha_{I}$ or 0.38 μg/ml $NaCh\alpha_{II}$), followed by ^{125}I-protein A. Blots were analyzed with a PhosphorImager; the specific ~200-kDa signals, corresponding to $NaCh\alpha_{I}$ and $NaCh\alpha_{II}$, were quantified using the ImageQuant software.

Hippocampal cultures

Newborns were placed under ice to induce hypothermia and then decapitated. Brains were removed and kept on ice in a divalent cation-free balanced saline solution (HBS): 144 mM NaCl, 3 mM KCl, 10 mM HEPES, pH 7.3. Hippocampi were dissected in ice-cold HBS solution and then incubated in Dulbecco's modified minimum essential medium (DMEM) (BioWhittaker) supplemented with 0.1% trypsin for 15 min at 37°C. Hippocampi were then washed twice in HBS and transferred to "complete medium," i.e., DMEM supplemented with Ham's F12 (BioWhittaker) and heat-inactivated bovine calf serum (Hyclone) (8:1:1 v/v), 24 U/ml penicillin, and 24 μg/ml streptomycin (Sigma). Tissue was triturated by repeated passings (≤10) through a fire-polished Pasteur pipette. Cells were counted in the presence of 0.04% Trypan blue and plated (~10^4 viable cells/cm^2) on poly-L-lysine-coated coverslips. Cultures were maintained on complete medium at 37°C in a humidified atmosphere containing 6% CO_2.

Electrophysiology

Neurons cultured for 5–9 days in vitro were used. The extracellular recording solution was 50 mM NaCl, 110 mM tetraethylammonium chloride, 2 mM $BaCl_2$, 0.3 mM $CdCl_2$, and 10 mM HEPES (pH 7.4). Whole-cell recordings (Hamill et al., 1981) were obtained at 23 ± 2°C, using pipettes pulled from Corning 7052 capillaries (Garner) on a P-97 puller (Sutter). Electrodes were filled with an internal solution containing 117 mM CsCl, 9 mM EGTA, 9 mM HEPES, 5 mM NaCl, 1.8 mM $MgCl_2$, 14 mM Tris-creatinePO_4, 4 mM MgATP, and 0.3 mM Tris-GTP (pH 7.4) (Raman et al., 1997). The pipette tip resistance was 5.5–7 MΩ. Access resistance (~20 MΩ) was compensated for by ~75%, and capacitative transients were minimized through the analog compensation circuitry of the patch-clamp amplifier (List EPC-7), which was also used to estimate cell capacity. Data were acquired and analyzed using an ITC-16 interface (Instrutech) and Pulse/PulseFit acquisition and analysis software (Heka). Currents were leak subtracted using the P/4 protocol. Processed data are reported as mean ± SE; *n* denotes the number of experiments. Statistical significance was assessed using Student's *t*-test.

Saxitoxin binding, autoradiography, and image analysis

Procedures were performed as described (Xia and Haddad, 1994). ^{3}H-Saxitoxin (^{3}H-STX) (24.0 Ci/mmol) and unlabeled STX were from Amersham and Calbiochem, respectively. Newborns were snap-frozen in isopentane cooled with liquid nitrogen. Frozen tissue blocks were mounted with OLR media and sectioned with a Leica cryostat. Frozen sections were incubated with ^{3}H-STX in STX binding buffer in the 10–24 nM concentration range. Nonspecific binding was estimated by the addition of excess cold STX. One set of sections was used for autoradiography and another was scraped and quantified in a scintillation counter.

Tissue processing and histological analysis

A total of 150 newborns, ~50 each of $NaCh\alpha_{II}^{+/+}$, $NaCh\alpha_{II}^{+/-}$, and $NaCh\alpha_{II}^{-/-}$ mice, were analyzed. Mice were placed in Bouin's fixative for 24 h, then divided sagitally and postfixed for 48 h. Specimens were washed, dehydrated, paraffin-embedded, serially sectioned at 7 μm with a

Leica microtome, and stained with hematoxylin and eosin (H&E) or cresyl violet. Subsets of paraffin sections were used for immunocytochemistry and terminal deoxynucleotidyl transferase-mediated dUTP nick-end labeling (TUNEL) staining.

Immunocytochemistry

Brain NaChα_{II} or NaChα_{I} subunits were localized by utilizing antibodies generated against peptides corresponding to residues 467–485 or 465–481 of the rodent proteins (Alomone) (Westenbroek et al., 1992), using 10-μm-thick paraffin sections (Masliah et al., 1998b). Blind-coded paraffin sections were first washed in sodium phosphate buffer, treated with H_2O_2, blocked with secondary antibody species-specific serum, and incubated overnight at 4°C with NaChα_{II} or NaChα_{I} antibodies. Sections were then washed and incubated with biotinylated goat anti-rabbit IgG, followed by avidin D horseradish peroxidase (ABC Elite, Vector Laboratories), and reacted with diaminobenzidine tetrahydrochloride containing 0.001% H_2O_2.

TUNEL assay and EM analysis of apoptosis

Cells undergoing DNA fragmentation were identified using a modified version (Masliah et al., 1998a) of the TUNEL method (Ben-Sasson et al., 1995). TdT-positive neurons were determined by image analysis and expressed as a mean per unit area. For EM, brains were fixed with 2% glutaraldehyde/0.1% osmium tetroxide in 0.1 M sodium cacodylate and embedded in epoxy. Blocks were sectioned with a Leica Ultracut E ultramicrotome, placed on copper grids, stained by the Sato lead method, and evaluated with a Zeiss EM10 electron microscope (Masliah et al., 1996).

RESULTS

Targeted disruption of the NaChα_{II} gene

The NaChα_{II} gene was inactivated by homologous recombination deleting most of exon 1, encoding from amino acid 1 to amino acid 89, and substituting this sequence by the neomycin resistance gene (*neo*^{r}) (Fig. 1 *A*). Two independently targeted ES cell lines, J1–87 and R1–34, were obtained, injected into C57BL/6J blastocysts, and transferred to pseudopregnant females. Three chimeric males from the R1–34 line gave germline transmission of the mutated NaChα_{II} gene. Southern blot analysis of wild type (WT) and the two successfully targeted ES cell clones is shown in Fig. 1 *B*. Confirmed chimeras were then crossed to C57BL/6J mice to generate heterozygous NaChα_{II} mutants, and heterozygous mice were then crossed to generate the homozygous NaCh$\alpha_{II}^{-/-}$ mice. Tail DNA from offspring mice were genotyped by PCR amplification, using two oligonucleotide primers flanking the *neo*^{r} insertion site. The WT locus amplified a band of 450 bp, whereas the targeted locus amplified a band of ~1.3 kb (Fig. 1 *C*). Southern blot analysis of the same tail genomic DNA digested with *Bgl*II, using an internal probe, confirmed the genotype (Fig. 1 *D*). Genotyping of more than 640 newborn pups derived from interbreeding of heterozygous mice indicated that the NaChα_{II} deficiency in the NaCh$\alpha_{II}^{-/-}$ mice resulted in peri-

natal lethality, despite a Mendelian distribution that suggests that the NaChα_{II} gene is not embryonic lethal (Table 1).

NaChα_{II} expression is drastically reduced in the brains of NaCh$\alpha_{II}^{-/-}$ mice

We investigated the expression of the NaChα_{II}. RNase protection assays revealed that the steady-state level of the NaChα_{II} transcript present in whole brain preparations of NaCh$\alpha_{II}^{-/-}$ and NaCh$\alpha_{II}^{+/-}$ mice was reduced by $\geq$85% and ~50% compared to that detected in brains of NaCh$\alpha_{II}^{+/+}$ littermates (Fig. 2 *A*). In contrast, RNase protection assays specific for the NaChα_{I} transcript showed no detectable differences between NaCh$\alpha_{II}^{-/-}$ and NaCh$\alpha_{II}^{+/-}$ mice.

To determine the relative levels of NaChα_{II} mRNA in different brain regions, brains from NaCh$\alpha_{II}^{-/-}$, NaCh$\alpha_{II}^{+/-}$, and NaCh$\alpha_{II}^{+/+}$ mice were dissected into cortex, hippocampus, and brainstem. This analysis showed that the brain region that expressed the highest NaChα_{II} transcript level was the brainstem, followed by hippocampus and neocortex. There was a drastic reduction of NaChα_{II} transcript level in NaCh$\alpha_{II}^{-/-}$ mice in all three brain regions and a reduction in the NaCh$\alpha_{II}^{+/-}$ mice with respect to wild type, ranging from ~36% in brainstem and ~48% in cortex to ~53% in hippocampus. The most striking feature appeared to be the ratio of transcript level between wild-type mice and the homozygous mutant (Δ), which followed the sequence brainstem ($\Delta \cong 6$) > cortex ($\Delta \cong 5$) > hippocampus ($\Delta \cong 4$) (Fig. 2 *B*). Statistical analysis of differences between the three groups of mice showed that differences between NaCh$\alpha_{II}^{+/+}$ and NaCh$\alpha_{II}^{+/-}$, between NaCh$\alpha_{II}^{+/+}$ and NaCh$\alpha_{II}^{-/-}$, and between NaCh$\alpha_{II}^{+/-}$ and NaCh$\alpha_{II}^{-/-}$ were significant at the $p < 0.05$ level (poshoc Fisher). These results suggest that the expression of NaChα_{II} RNA is dosage sensitive and most drastically compromised in the brainstem of the NaCh$\alpha_{II}^{-/-}$ neonates.

To verify that the reduction of NaChα_{II} mRNA expression in the NaCh$\alpha_{II}^{-/-}$ mice was associated with a concomitant reduction in protein expression, levels of NaChα_{II} immunoreactivity were determined by protein immunoblot analysis (Westenbroek et al., 1992) (Fig. 2 *C*). In brain membranes from NaCh$\alpha_{II}^{+/+}$ and NaCh$\alpha_{II}^{+/-}$ mice NaChα_{II} immunoreactivity was discernible as an intense band at a M_r of ~200 kDa, whereas in membranes from NaCh$\alpha_{II}^{-/-}$ mice NaChα_{II} immunoreactivity was barely detectable. In contrast, NaChα_{I} protein was detected at approximately the

TABLE 1 Survival of progeny from heterozygous intercrosses

		NaCh$\alpha_{\parallel}$ genotype frequency		
Viability	No. of litters	+/+	+/−	−/−
At birth	86	218	273	149
Two days after birth	86	218	273	0

FIGURE 2 Analysis of NaChα$_{II}$ mRNA levels in brains of NaChα$_{II}^{-/-}$ mice. (A) Representative RPA autoradiograph. The lane identified as Probe shows signals of undigested radiolabeled probes (indicated on the *left*; no RNase added). The other lanes contained the same riboprobes and brain RNA samples from newborn littermates and adult NaChα$_{II}^{+/+}$ and NaChα$_{II}^{+/-}$ mice, digested with RNase. Labels and arrows on right indicate the expected size for specific protected mRNA fragments after digestion of noncomplementary sequences (vector-derived) and transcripts. Actin signals were used as a control for RNA content/loading. (B) PhosphorImager quantitation of RPAs conducted on hippocampus, cortex, and brainstem from NaChα$_{II}^{+/+}$, NaChα$_{II}^{+/-}$, and NaChα$_{II}^{-/-}$ littermates. Columns and error bars represent means ± SE (*n* = 3). (C) Western blot analysis of NaChα$_I$ and NaChα$_{II}$ immunoreactivity from brain membranes of NaChα$_{II}^{+/+}$, NaChα$_{II}^{+/-}$, and NaChα$_{II}^{-/-}$ littermates. Lanes labeled "rat" indicate positive control preparations obtained from rodent brains. Numbers indicate M_r standards. Anti-NaChα$_I$ and anti-NaChα$_{II}$ indicate blots probed with the corresponding antibody. Nonspecific background and cross-reactivity of anti-NaChα$_{II}$ to NaChα$_{III}$ may account for the dim bands present in the NaChα$_{II}^{-/-}$ samples.

same levels in membranes from NaChα$_{II}^{+/+}$, NaChα$_{II}^{+/-}$, and NaChα$_{II}^{-/-}$ mice. Together, these results are consistent with the RNase protection data and show that NaChα$_{II}$ protein expression is markedly reduced in brains of NaChα$_{II}^{-/-}$ mice.

Sodium channel currents in hippocampal neurons of NaChα$_{II}^{-/-}$ mice are sharply attenuated

We investigated the biophysical properties of NaChs, using whole-cell recordings from hippocampal neurons in culture (Hamill et al., 1981). Fig. 3 *A* (*left*) shows families of sodium currents in response to a series of 20-ms depolarizing voltage steps, from a holding potential of −120 mV, for NaChα$_{II}^{+/+}$ (*top*), NaChα$_{II}^{+/-}$ (*middle*), and NaChα$_{II}^{-/-}$ (*bottom*) mice. The time course of the current transients is characteristic of voltage-gated NaChs (Armstrong and

Hille, 1998): currents increase to a peak and then decline with a sigmoidal early activation and a subsequent exponential decay. The peak current-voltage (*I-V*) relationship is shown in the corresponding right panels. The most conspicuous feature was the drastic reduction of *I* in cells from the NaChα$_{II}^{-/-}$ mice. On average, the maximum conductance (G_{max}) density, determined from the positive resistance region of the *I-V* curve, was 0.33 ± 0.05 (*n* = 15), 0.64 ± 0.06 (*n* = 45), and 1.12 ± 0.13 nS/pF (*n* = 26) for cells from NaChα$_{II}^{-/-}$, NaChα$_{II}^{+/-}$, and NaChα$_{II}^{+/+}$ mice, respectively (Fig. 3 *B*). The differences between the three groups were statistically significant ($p < 0.001$). This pattern of expression of sodium currents follows gene dosage and is consistent with the findings of the RNase protection assay and protein immunoblots, all indicative of a severe deficiency of the NaChα$_{II}$ gene product. The residual sodium currents in cells from the NaChα$_{II}^{-/-}$ mice is consistent with
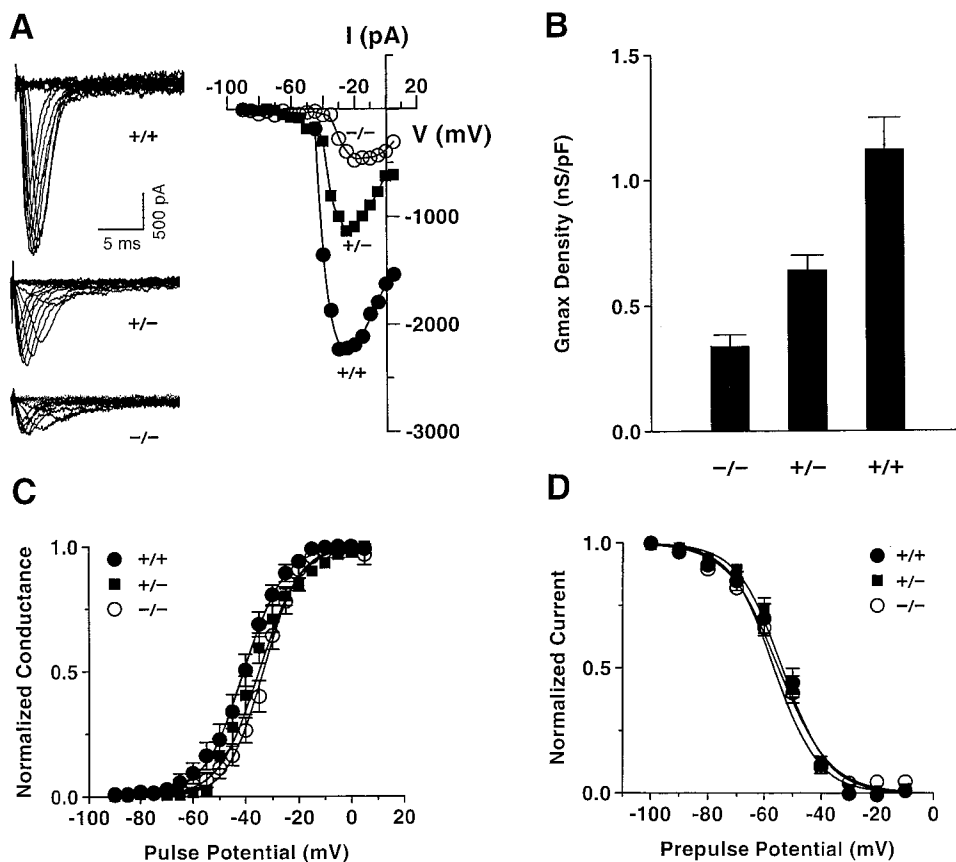
FIGURE 3   Sodium channel currents in hippocampal pyramidal neurons from newborn NaCh$\alpha_{II}^{+/+}$, NaCh$\alpha_{II}^{+/-}$, and NaCh$\alpha_{II}^{-/-}$ littermates. (*A*) Family of sodium currents elicited by 20-ms voltage steps from a holding potential of -120 mV. Test potentials ranged from -90 mV to 5 mV in 5-mV increments. Time and current scale bars apply to all three left panels. Right panels show the peak currents plotted versus test potential for the records shown at left. (*B*) Maximum sodium conductance (G_{max}) density evoked by depolarizing potentials for neurons from NaCh$\alpha_{II}^{+/+}$ ($n = 26$), NaCh$\alpha_{II}^{+/-}$ ($n = 45$), and NaCh$\alpha_{II}^{-/-}$ ($n = 15$) littermates. Columns and error bars represent means $\pm$ SE. (*C*) Peak conductance-voltage (G_{peak}-*V*) relationships calculated according to $G_{peak} = I_{peak}/(V - V_{Na+})$, where *I* is the peak current amplitude, *V* is the applied voltage, and V_{Na+} is the Nernst equilibrium potential. The solid line depicts the least-squares fit to data points and is given by a Boltzmann function, normalized $G = 1/\{1 + \exp(-(V - V_{1/2})/a)\}$, where $V_{1/2}$ is the half-activation potential at which the slope *a* is depicted. The $V_{1/2}$ and *a* values for the fitted curves are -40.7 mV ($n = 12$) and 7.7 for NaCh$\alpha_{II}^{+/+}$ ($n = 25$), -35.0 mV and 7.6 for NaCh$\alpha_{II}^{+/-}$ ($n = 45$), and -33.5 mV and 6.8 for NaCh$\alpha_{II}^{-/-}$ ($n = 14$). Each point represents the mean $\pm$ SE. (*D*) Steady-state voltage dependence of inactivation, determined using a series of 200-ms prepulses, ranging from -100 mV to -10 mV, followed by a 10-ms test pulse to 0 mV. Peak currents were normalized with respect to the maximum and plotted as a function of the prepulse potential. The solid line plots the least-squares fit to the data points given by a Boltzmann function, Normalized current $= 1/\{1 + \exp(-(V - V_h)/a)\}$, where *V* is the prepulse potential and V_h is the half-inactivation potential at which the slope *a* is depicted. The V_h and *a* values for the fitted curves are -53.6 mV and 8.1 for NaCh$\alpha_{II}^{+/+}$ ($n = 15$), -56.5 mV and 7.9 for NaCh$\alpha_{II}^{+/-}$ ($n = 20$), and -54.9 mV and 9.0 for NaCh$\alpha_{II}^{-/-}$ ($n = 9$). Each point represents the mean $\pm$ SE.

the occurrence of other NaChs, the expression of which is not altered by the targeted disruption of the NaChα_{II} gene.

The currents were characterized by examining the peak sodium conductance-voltage relation (*G-V*) (Fig. 3 *C*). The *G-V* curve is a sigmoidal function of voltage, which is taken as an indication of the relative number of channels that are closed versus open as a function of voltage. The solid lines depict the least-squares fit of the data to the Boltzmann function reported in Fig. 3; two parameters were extracted from the fit: $V_{1/2}$, the half-activation potential at which the slope *a* is depicted. For the NaCh$\alpha_{II}^{+/+}$, *G* increased with depolarizing voltages to a maximum at a $V \approx -10$ mV, exhibiting a $V_{1/2}$ at $V = -40.7$ mV and an *e*-fold change in

G per 7.7 mV. The corresponding parameters for the NaCh$\alpha_{II}^{+/-}$ and NaCh$\alpha_{II}^{-/-}$ were $V_{1/2} = -35.0$ mV and -33.5 mV, with an *e*-fold change in *G* per 7.6 mV and 6.8 mV, respectively. Statistical analysis of the data shows that the $V_{1/2}$ values are -40.3 ± 2.2 mV ($n = 25$), -34.6 ± 1.2 mV ($n = 46$), and -32.8 ± 1.8 mV ($n = 14$) for NaCh$\alpha_{II}^{+/+}$, NaCh$\alpha_{II}^{+/-}$, and NaCh$\alpha_{II}^{-/-}$ neurons, respectively. The positive shift of 7.5 mV in the NaCh$\alpha_{II}^{-/-}$ mice with respect to the NaCh$\alpha_{II}^{+/+}$ littermates is statistically significant ($p = 0.025$), whereas the difference in $V_{1/2}$ values between NaCh$\alpha_{II}^{+/-}$ and NaCh$\alpha_{II}^{-/-}$ neurons is not ($p = 0.47$). Thus the remaining ensemble of NaChs in hippocampi of NaCh$\alpha_{II}^{-/-}$ mice activates at more positive voltage.

The steady-state voltage dependence of inactivation was studied by using a pulse protocol in which the test pulse to 0 mV was preceded by 200-ms depolarizing prepulses to different potentials (Fig. 3 D). As the potential of the prepulse is increased, the current flow during the test pulse decreases sigmoidally because of the voltage-dependent inactivation of channels during the prepulse. For the $NaCh\alpha_{II}^{+/+}$, the midpoint of the steady-state inactivation (V_h), extracted from a fit of the data points to a Boltzmann function, was -53.6 mV, with an e-fold decrease in the steady-state state current per 8.0 mV. The corresponding parameters for the $NaCh\alpha_{II}^{+/-}$ and $NaCh\alpha_{II}^{-/-}$ were $V_h = -56.5$ mV and -54.9 mV, with an e-fold change in G per 7.9 mV and 9.0 mV. Statistical analysis of the data shows that the V_h values are -52.3 ± 2.3 mV ($n = 15$), -58.1 ± 1.6 mV ($n = 20$), and -54.7 ± 1.4 mV ($n = 9$) for $NaCh\alpha_{II}^{+/+}$, $NaCh\alpha_{II}^{+/-}$, and $NaCh\alpha_{II}^{-/-}$ neurons, respectively. The difference in V_h values between the three groups is not statistically significant ($p > 0.1$). Together, these results show that the targeted disruption

of $NaCh\alpha_{II}$ reduces the NaCh currents in hippocampal neurons with minor changes in the equilibrium voltage-dependent properties.

The density of saxitoxin-binding sites is markedly reduced in the rostral brain and barely detectable in the brainstem of $NaCh\alpha_{II}^{-/-}$ mice

To determine the density of NaChs in brains from $NaCh\alpha_{II}^{-/-}$ mice we used saxitoxin (STX), a specific ligand of voltage-gated NaCh α subunits (Xia and Haddad, 1994; Couraud et al., 1986). Autoradiographic analysis of brain sections exposed to ^{3}H-STX showed that the STX binding density was markedly reduced in the rostral brain and in the brainstem of the $NaCh\alpha_{II}^{-/-}$ mice (Fig. 4, C and D). This finding is to be contrasted with the high STX binding density in the brainstem of $NaCh\alpha_{II}^{+/+}$ littermates (Fig. 4, A and D). The slight increment in STX binding affinity dis-
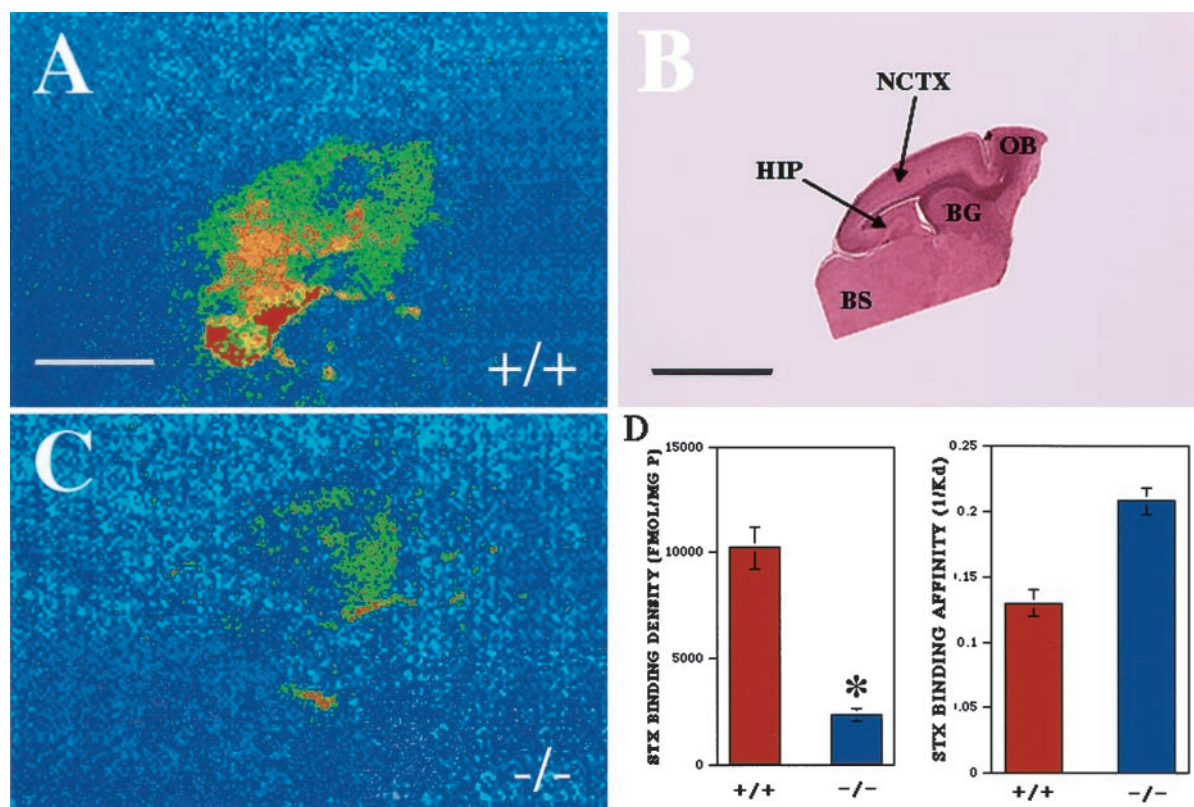

FIGURE 4   Marked reduction in STX-binding density in the brainstem of $NaCh\alpha_{II}^{-/-}$ mice. Autoradiographic images from brains of $NaCh\alpha_{II}^{+/+}$ (A) and $NaCh\alpha_{II}^{-/-}$ (C) newborn littermates are pseudocolored to represent the relative STX binding density, from highest (*red*) to lowest (*blue*). Autoradiograms were obtained at 15 nM ^{3}H-STX. (B) Comparable brain section stained with H&E, indicating selected regions: OB, olfactory bulb; NCTX, neocortex; BG, basal ganglia; HIP, hippocampus; BS, brainstem. (A) Autoradiograms of $NaCh\alpha_{II}^{+/+}$ brains show the most intense binding in the brainstem, followed by the hippocampus and basal ganglia; the olfactory bulb and neocortex display lower binding. (C) Autoradiograms of $NaCh\alpha_{II}^{-/-}$ brains show very weak STX binding in the brainstem and modest binding in the basal ganglia and neocortex. Magnification for A–C: 10×. Scale bar, 3 mm. (D) Quantitation of STX binding density and affinity in brains of $NaCh\alpha_{II}^{+/+}$ and $NaCh\alpha_{II}^{-/-}$ newborn littermates. STX binding affinity is expressed as $1/K_d$. Statistical significance was assessed using the unpaired, two-tailed Student t-test; the asterisk indicates that the differences are statistically significant with $p < 0.05$. Columns and error bars represent means $\pm$ SE ($n = 3$).

played by NaChα$_{II}^{-/-}$ mice suggests that the remaining aggregate of NaChs was not altered (Fig. 4 *D*).

It is known that *SCN1A* (Smith et al., 1998)*, SCN2A* (Noda et al., 1986; Suzuki et al., 1988; Smith et al., 1998)*, SCN3A* (Suzuki et al., 1988), and *SCN8A* (Smith et al., 1998) α subunits bind tetrodotoxin and STX with comparable affinities. It is therefore unlikely that the modest increase in STX binding affinity detected in brains from NaChα$_{II}^{-/-}$ newborn mice arises from a higher affinity of the remaining aggregate of NaChs. Subtle differences in affinity, discerned by using this type of global measurement (Xia and Haddad, 1994), may reflect the relative abundance of the remaining NaCh in the newborn brain of NaChα$_{II}^{-/-}$ mice. It is known that the different NaCh α subunit mRNAs display distinct temporal expression patterns in the CNS (Beckh et al., 1989). *SCN2A* is the most abundant species postnatally and remains at high levels through adulthood (Beckh et al., 1989). *SCN3A* is expressed predominantly at fetal and early postnatal stages, whereas *SCN1A* predominates at late postnatal stages (Beckh et al., 1989). No comparable information is available for *SCN8A*; however, the development and function of spinal motoneurons depends on the postnatal induction of *SCN8A* expression (Garcia et al., 1998). Based on the information at hand, it is conceivable that, in the absence of the most abundant *SCN2A* (Beckh et al., 1989), the preponderant species in newborn brains is *SCN3A,* and that the modest increase in STX binding affinity measured in NaChα$_{II}^{-/-}$ newborn brains is nothing more than a reflection of this enrichment relative to *SCN1A* and *SCN8A*.

Perinatal lethality of NaChα$_{II}^{-/-}$ mice

Mice heterozygous for the mutation (NaChα$_{II}^{+/-}$) appeared to be normally developed and did not display gross morphological anomalies. In contrast, NaChα$_{II}^{-/-}$ pups died within 1–2 days of birth. During this early postnatal period, the pups appeared to quickly dehydrate and lose weight (~16% lower body weight than NaChα$_{II}^{+/-}$ littermates, measured concurrently within 12 h of birth); they were pallid, dyspneic or gasping, and cyanotic (Fig. 5 *A*). The lower abdominal region was dark, with reduced milk content in the stomach. NaChα$_{II}^{-/-}$ neonates were hypoxic and presented a drastic reduction of the hemoglobin percentage saturation (59 ± 5%, $n = 9$), contrasted with NaChα$_{II}^{+/+}$ (86 ± 4%, $n = 7$) and NaChα$_{II}^{+/-}$ littermates (83 ± 4%, $n = 7$). No seizure activity was detected in NaChα$_{II}^{-/-}$ neonates; pups move and react to gentle touch without an apparent difference with respect to NaChα$_{II}^{+/-}$ littermates.

Despite the severe deficiency of NaChα$_{II}$, the identification of residual NaChα$_{II}$ mRNA and protein (Fig. 2) suggests that the targeted disruption of the NaChα$_{II}$ gene may be incomplete. Arguably, NaChα$_{II}^{-/-}$ mice do not express sufficient levels of NaChα$_{II}$ to allow survival to adulthood. In contrast, the NaChα$_{II}^{+/-}$ mice breed normally and appear

to be functional. Clearly, levels of NaChα$_{II}$ somewhere between these two boundaries are required for survival.

Absence of neuroanatomical alterations in NaChα$_{II}^{-/-}$ mice

Inspection of brains from NaChα$_{II}^{-/-}$ newborn mice revealed no neuroanatomical abnormalities. Microscopic analysis of the cortical (Fig. 5, *B–D*), hippocampal (Fig. 5, *E–G*), cerebellar, and brainstem regions showed these to be well developed, comparable to those of the NaChα$_{II}^{+/+}$ and NaChα$_{II}^{+/-}$ littermates, exhibiting overall intact organization and well-defined neuronal cytoarchitectures. Immunocytochemical analysis of neonate brains from NaChα$_{II}^{+/+}$ and NaChα$_{II}^{+/-}$ mice revealed anti-NaChα$_{II}$ immunoreactivity associated with the neuronal cell bodies. Pyramidal neurons in the neocortex and hippocampus showed mild immunoreactivity, whereas neurons within the brainstem and dorsal root ganglion presented intense anti-NaChα$_{II}$ immunoreactivity (Fig. 5 *H*). In the NaChα$_{II}^{-/-}$ mice there was a marked reduction of NaChα$_{II}$ immunoreactivity throughout the nervous system, as shown in a representative section of brainstem (Fig. 5 *I*). The NaChα$_{I}$-specific antibody reacted mildly with neuronal cell bodies throughout the CNS of NaChα$_{II}^{+/+}$, NaChα$_{II}^{+/-}$, and NaChα$_{II}^{-/-}$ mice. No differences were discerned, as displayed in representative sections of brainstem (Fig. 5, *J* and *K*) for NaChα$_{II}^{+/+}$ and NaChα$_{II}^{-/-}$ mice, respectively.

Increased neuronal apoptosis and death in neurons of NaChα$_{II}^{-/-}$ mice

Given that organogenesis and brain development appeared to be normal in the NaChα$_{II}^{-/-}$ mice, and considering that neonates die within 24–48 h of birth with a severe hypoxic phenotype, we hypothesized that abnormal neuronal function compromised by the NaChα$_{II}$ deficit might lead to neuronal cell death, especially in brain areas critically involved in respiratory regulation. To test this model, analysis of neuronal cell death was undertaken, using the TUNEL method (Ben-Sasson et al., 1995). A most conspicuous phenotype of the NaChα$_{II}^{-/-}$ mice is the marked increment in neuronal apoptosis in the brainstem (Fig. 6, *D* and *F*). On average, 4.5-fold and 3-fold increments in the number of TUNEL-positive cells per section were identified in the brainstem (Fig. 6, *D* and *F*) and neocortex (Fig. 6, *B* and *E*) from NaChα$_{II}^{-/-}$ mice. This is consistent with a global change of the brain, presumably associated with the hypoxia identified in NaChα$_{II}^{-/-}$ neonates.

To determine whether the positive TUNEL reaction was due to augmentation of apoptosis or to necrotic changes secondary to hypoxia, tissues were prepared for ultrastructural examination. This analysis revealed that neurons from the NaChα$_{II}^{-/-}$ mice presented a marked increase in chro-

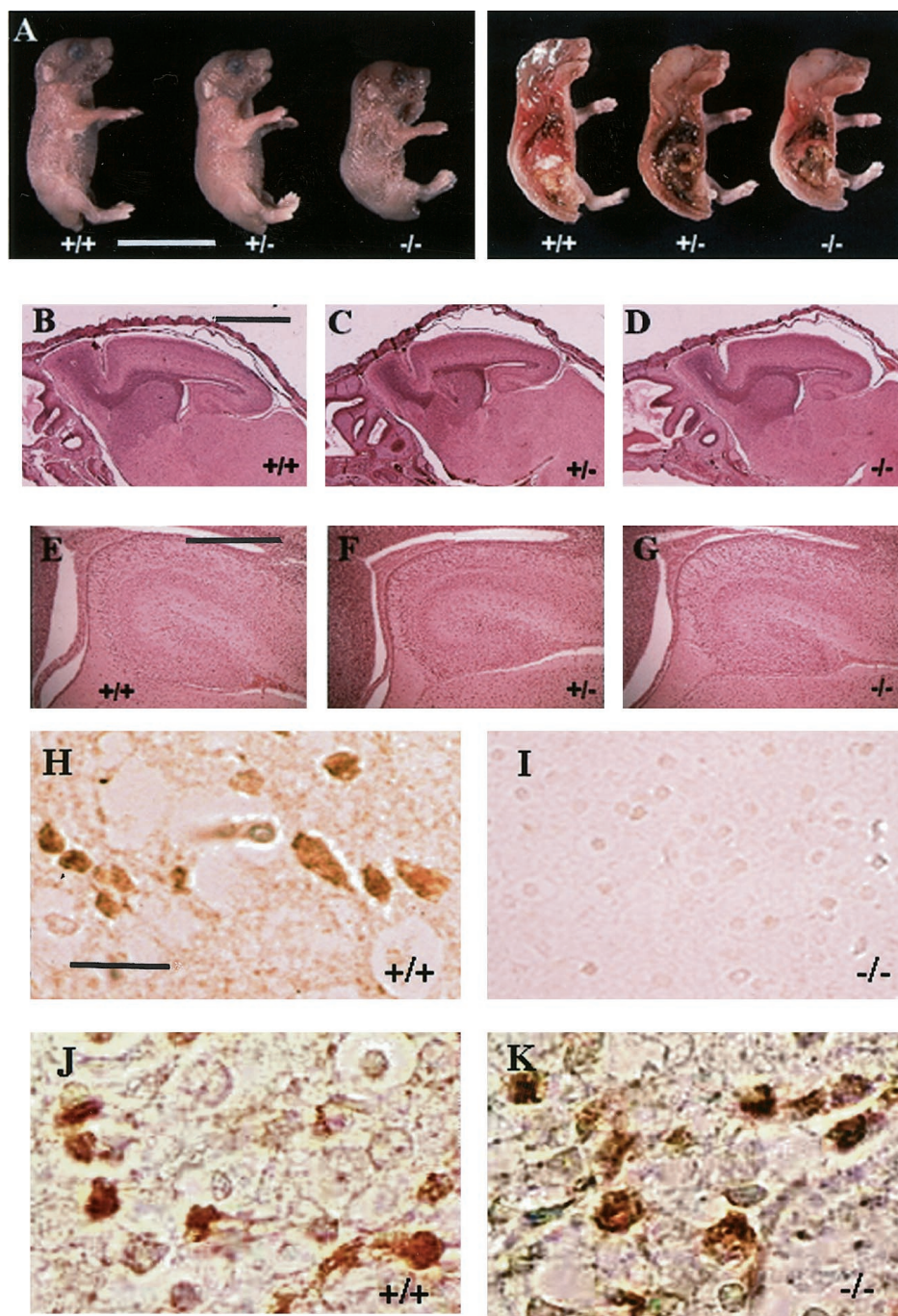FIGURE 5 Anatomical analysis of $\mathrm{NaCh}\alpha_\mathrm{II}^{-/-}$ mice. (*A*) Gross examination of the $\mathrm{NaCh}\alpha_\mathrm{II}^{+/+}$, $\mathrm{NaCh}\alpha_\mathrm{II}^{+/-}$, and $\mathrm{NaCh}\alpha_\mathrm{II}^{-/-}$ mice shows normal organogenesis; $\mathrm{NaCh}\alpha_\mathrm{II}^{-/-}$ mice appear smaller in size. Scale bar, 10 mm. (*B–D*) Neurohistological examination of H&E-stained forebrain (*top panels*; magnification 20×; scale bar, 2 mm) and hippocampus (*bottom panels*, magnification 40×; scale bar, 0.5 mm) of $\mathrm{NaCh}\alpha_\mathrm{II}^{+/+}$ (*B*), $\mathrm{NaCh}\alpha_\mathrm{II}^{+/-}$ (*C*), and $\mathrm{NaCh}\alpha_\mathrm{II}^{-/-}$ (*D*) mice shows normal development. (*H–K*) Analysis of patterns of $\mathrm{NaCh}\alpha_\mathrm{II}$ (*H* and *I*) and $\mathrm{NaCh}\alpha_\mathrm{I}$ (*J* and *K*) immunoreactivity in the CNS revealed intense $\mathrm{NaCh}\alpha_\mathrm{II}$ immunoreactivity in the brainstem (*H*) of $\mathrm{NaCh}\alpha_\mathrm{II}^{+/+}$ mice, contrasted to the lack of neuronal staining in the corresponding brain region of the $\mathrm{NaCh}\alpha_\mathrm{II}^{-/-}$ mice (*I*). No differences in $\mathrm{NaCh}\alpha_\mathrm{I}$ immunoreactivity between the brainstems of $\mathrm{NaCh}\alpha_\mathrm{II}^{+/+}$ (*I* and *J*) and $\mathrm{NaCh}\alpha_\mathrm{II}^{-/-}$ (*K*) mice were detected. Sections were obtained from mice ~12 h after birth. Magnification, 263×. Scale bar, 20 μm.

matin condensation and segregation (Fig. 7, *B* and *D–F*), two prominent features of apoptotic neurons (Portera-Cailliau et al., 1997). Mitochondria appeared to be markedly swollen, with cristae dilatation, in neurons from brains of $\mathrm{NaCh}\alpha_\mathrm{II}^{-/-}$ mice (Fig. 7 *D*) when compared with $\mathrm{NaCh}\alpha_\mathrm{II}^{+/+}$ littermates (Fig. 7 *C*). Complete condensation of chromatin and apoptotic bodies was clearly discerned in neurons from the $\mathrm{NaCh}\alpha_\mathrm{II}^{-/-}$ neonates (Fig. 7, *E* and *F*). In addition, the neuropil and neuronal cell bodies displayed extensive vacuolation. The areas most affected were the neocortex and

the brainstem. Thus neurons from $\mathrm{NaCh}\alpha_\mathrm{II}^{-/-}$ neonates display the ultrastructural hallmarks of apoptotic cell death.

DISCUSSION

We have generated knockout mice deficient in brain $\mathrm{NaCh}\alpha_\mathrm{II}$ that exhibit perinatal lethality with massive neuronal apoptosis. A most striking feature emerging from the biophysical analysis of NaCh currents from hippocampal
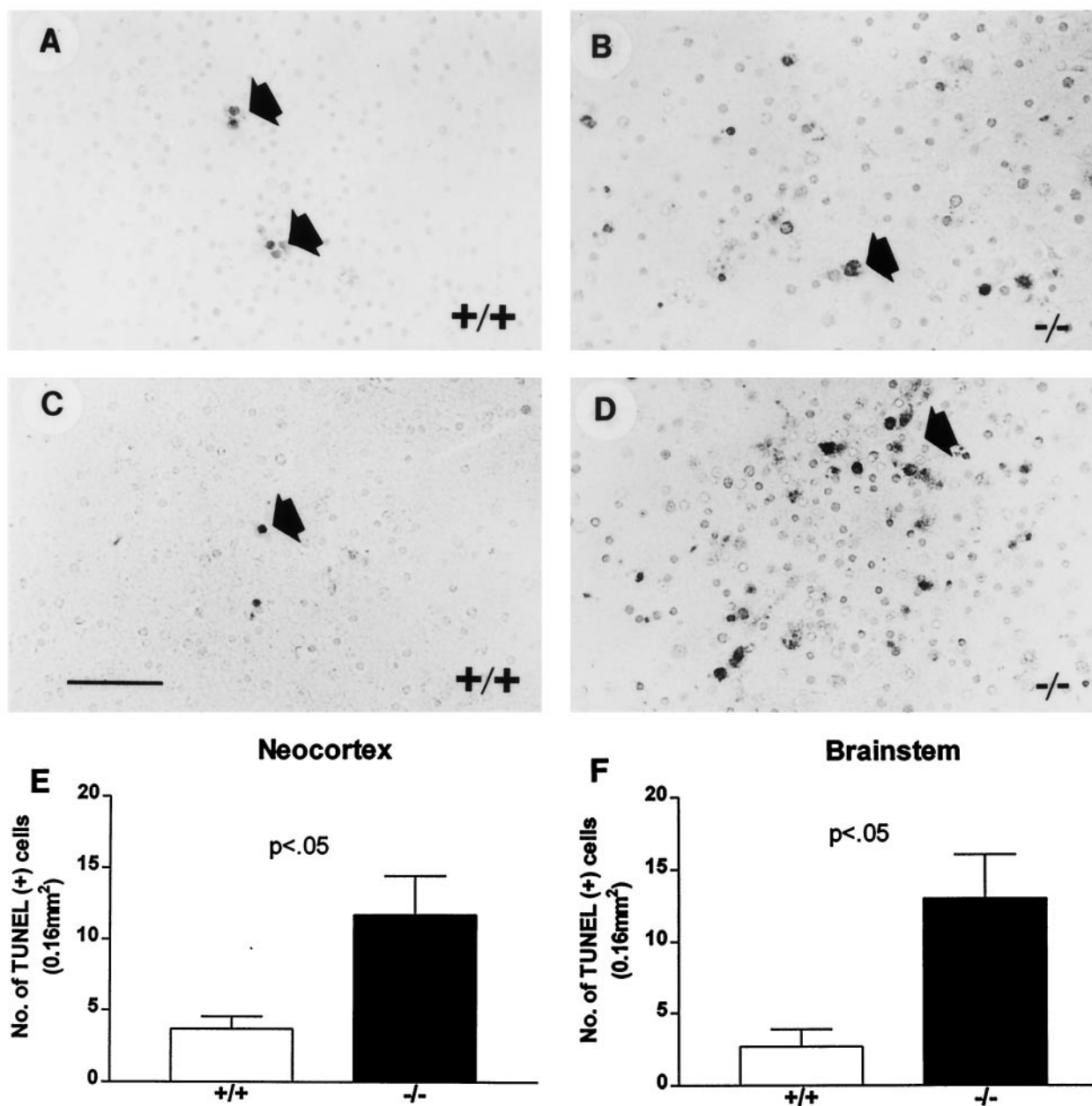
FIGURE 6 Increased neuronal apoptosis in the brains of NaCh$\alpha_{II}^{-/-}$ mice: in situ DNA fragmentation assay for apoptosis. In the wild-type neocortex (*A* and *E*) and brainstem (*C* and *F*), occasional labeling was discerned. In the neocortex (*B* and *E*) and brainstem (*D* and *F*) of NaCh$\alpha_{II}^{-/-}$ mice, extensive positive staining for apoptosis was observed (*arrows*). Magnification, 263×. Scale bar, 150 μm. Statistical significance was assessed using the unpaired, two-tailed Student's *t*-test ($p < 0.05$, $n = 3$).

neurons is the drastic reduction in the expression of sodium currents in the NaCh$\alpha_{II}^{-/-}$ mice. This, in and of itself, would explain the severe decrement in excitability apparent in the NaCh$\alpha_{II}^{-/-}$ mice. The electrophysiological analysis further uncovered the occurrence of a statistically significant depolarizing shift of 7.5 mV of the half-activation potential in the NaCh$\alpha_{II}^{-/-}$ mice with respect to the NaCh$\alpha_{II}^{+/+}$ littermates, contrasted with the invariance of the midpoint of the steady-state inactivation. Based solely on these characteristics,

neurons from the NaCh$\alpha_{II}^{-/-}$ mice would be expected to display decreased electrical excitability and a higher threshold for activation of action potentials compared with wild-type neurons. Such properties would produce a significant decrease in the probability of the channels that open in response to a given depolarization compared to neurons from wild-type animals, which would express the full complement of the NaChs. It is worth noting that these properties would be expected to lessen the window of excitability,
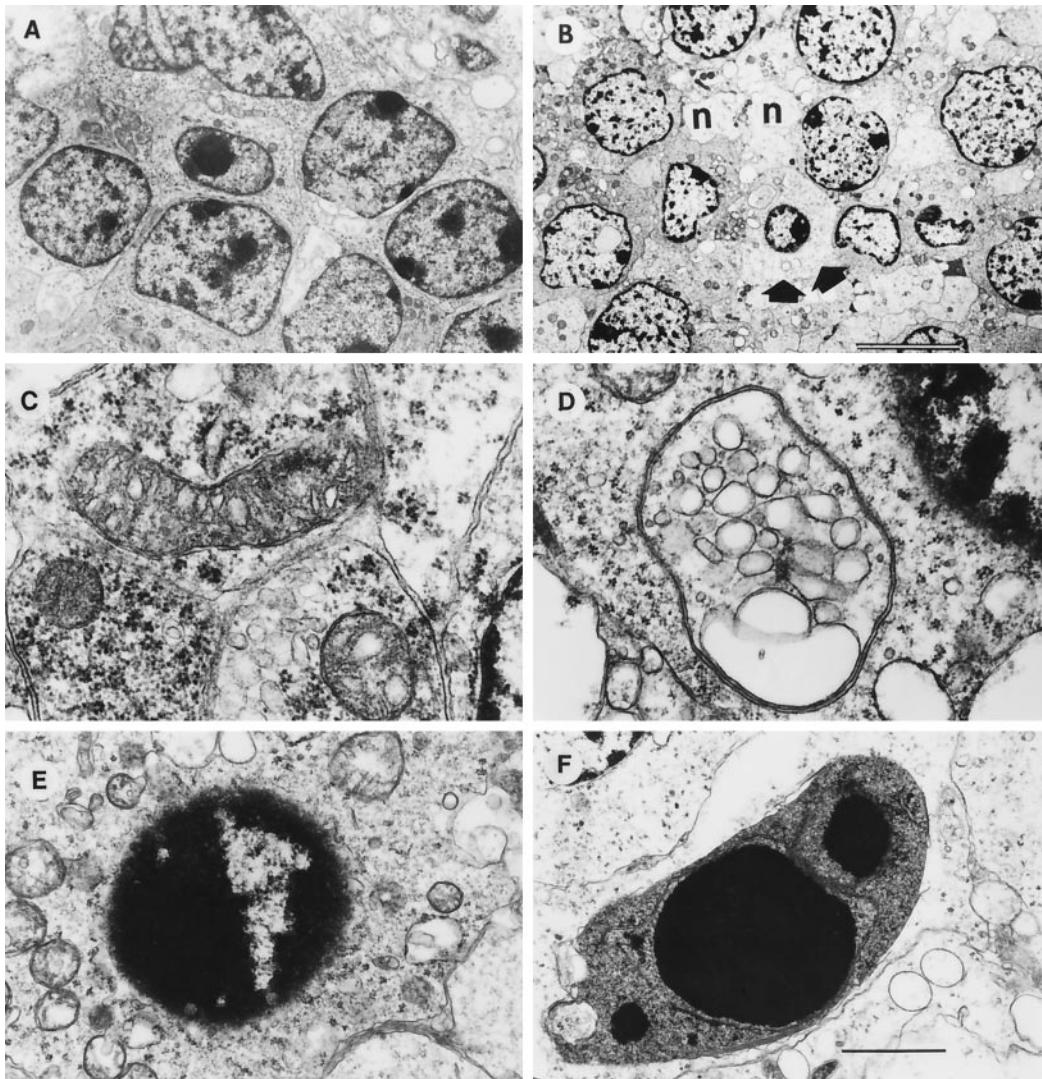
FIGURE 7 Ultrastructural analysis of neuronal alterations in the brains of $NaCh\alpha_{II}^{-/-}$ mice. (*A*) In $NaCh\alpha_{II}^{+/+}$ mice, neurons displayed a typical appearance. (*B*) In $NaCh\alpha_{II}^{-/-}$ mice, neurons exhibited extensive vacuolation of the cytoplasm (*arrows*) and the neuritic processes (n), accompanied by chromatin condensation. (*C*) In $NaCh\alpha_{II}^{+/+}$ mice, mitochondria displayed a normal appearance. (*D*) In $NaCh\alpha_{II}^{-/-}$ mice, mitochondria were swollen and their cristae were dilated. In addition, neurons displayed several levels of chromatin condensation, progressing from partial segmentation (*E*) to complete condensation (*F*). Magnification: *A* and *B*, 5000×; scale bar, 10 μm. *C* and *D*, 18,000×; scale bar, 10 μm. *E* and *F*, 10,000×; scale bar, 5 μm.

namely the net conductance that would occur in the voltage region where the activation and inactivation curves overlap. This is significant, as it has been documented that small changes in this "window current" are associated with channel dysfunctions or channelopathies. A case in point is hyperkalemic periodic paralysis, in which a mutation (T704M) of the human muscle NaCh α subunit (*SCN4A*) that is associated with the phenotype, when introduced into the recombinant channel and heterologously expressed, exhibits shifts in the midpoints of the steady-state activation and inactivation curves. The augmented overlap of the steady-state activation and inactivation curves would be expected to produce such a window current, which in turn would account for the persistent depolarizing inward so-

dium current across the muscle cells in patients with this disease (Yang et al., 1994).

The differences described between $NaCh\alpha_{II}^{+/+}$ and $NaCh\alpha_{II}^{-/-}$ neurons are likely to arise from the properties of the remaining NaChs, *SCN1A, SCN3A,* and *SCN8A*. The properties of heterologously expressed *SCN1A* (Smith et al., 1998) and *SCN3A* (Suzuki et al., 1988) appear to be fundamentally similar to those of *SCN2A* (Stuhmer et al., 1987, 1989; McCormick et al., 1999). It is documented that *SCN8A* channels inactivate more rapidly than *SCN1A* or *SCN2A* when expressed in amphibian oocytes (Smith et al., 1998). However, the three NaChs, *SCN1A, SCN2A,* and *SCN8A*, displayed similar voltage dependence and inactivation kinetics when coexpressed together with the β_1 and β_2

subunits (Smith et al., 1998). Presumably, the targeted deletion of the NaChα_{II} subunit in the mice reported here did not alter the expression of the β_1 and β_2 subunits. And it is most likely that sodium channels in the CNS are heterooligomers of α and β subunits. It is plausible, therefore, that the findings obtained with neurons from NaCh$\alpha_{II}^{-/-}$ mice arise from the remaining ensemble of NaChs assembled from combinations of *SCN1A, SCN3A,* and *SCN8A* α subunits with both β_1 and β_2 subunits.

There are several possible mechanisms by which the elimination of a single constituent from a multicomponent combination may give rise to the properties remaining in the system. First, the component missing in the NaCh$\alpha_{II}^{-/-}$ mice would accordingly be interpreted to exhibit a more negative midpoint of the steady-state activation than the residual components, *SCN1A, SCN3A,* and *SCN8A.* Evidence at hand suggests that this may be the case (Smith et al., 1998). Second, the possibility arises that deletion of the NaChα_{II} subunit induces compensatory up- or down-regulation of *SCN1A, SCN3A,* and *SCN8A,* by eliminating the competition of the remaining α subunits for the available complement of β_1 and β_2 subunits. Third, the absence of *SCN2A* may affect the interaction of the *SCN1A, SCN3A,* and *SCN8A* α subunits with the β subunits and thereby modulate the extent of surface expression of functional channels (Isom et al., 1995; Patton et al., 1994). Fourth, there may be accessory proteins other than both β subunits that may modulate the properties of the residual channels. For example, *SCN2A* channels display persistent currents when co-expressed with the G-protein $\beta\gamma$ subunits (Ma et al., 1997). It would be interesting to explore other possible mechanisms that may involve changes in protein trafficking or even gene expression arising from the interplay of NaCh α and β subunits with other protein components involved in synaptic activity, as has been suggested for calcium channels (Sutton et al., 1999).

The present study shows that although expression of NaChα_{II} is redundant for embryonic development, it is essential for postnatal survival. There are at least two plausible explanations for this finding. One view is that decreased neuronal activity associated with NaCh deficits activates programmed cell death within vital regions of the brain such as the brainstem and, in turn, leads to respiratory depression, hypoxia, and perinatal death. Alternatively, decreased neural activity within the brainstem may produce respiratory depression, hypoxia, oxidative stress, and secondary cell death. A sharp boundary between these two possible mechanisms may not occur, and the two may converge and contribute to neuronal demise and perinatal death. We tend to favor the first hypothesis, based on the following evidence. It is well documented that hypoxia alone is capable of inducing apoptosis in neuronal cultures and that the extent of damage is influenced by the duration and the severity of the hypoxic insult (Banasiak and Haddad, 1998). Furthermore, in this study we demonstrate

that the highest level of expression for NaChα_{II} is within the mouse brainstem neurons, in agreement with previous studies on rat brain (Xia and Haddad, 1994). The brainstem, the most primitive region of the brain, contains the respiratory rhythmogenic neurons and cardiovascular control centers, among others primarily involved in autonomic functions (St-John, 1998; Reckling and Feldman, 1998). The basic neuronal circuits that generate respiratory rhythm in the brainstem have been identified; however, the mechanisms of respiratory rhythmogenesis are still poorly understood (Reckling and Feldman, 1998; Gray et al., 1999). A site in the rostral ventrolateral medulla known as the pre-Bötzinger complex is considered to be necessary and sufficient to generate respiratory rhythm (Reckling and Feldman, 1998; Gray et al., 1999). And numerous distinct types of neurons have been identified in this complex; however, their functional phenotype, e.g., rhythm-generating or pattern-forming, remains to be defined. Despite the paucity of information, electrophysiological analysis of the properties of different neurons in this complex has disclosed the occurrence of neurons with intrinsic oscillatory bursting properties, associated to some extent with the activity of voltage-gated NaChs (Smith et al., 1992; Onimaru and Homma, 1992; Reckling et al., 1996). The abundance of NaChα_{II} in the brainstem makes it a plausible candidate, endowing a given class of rhythmogenic neurons with their bursting properties. The underlying mechanisms that determine that neurons within this brain region express high levels of NaChα_{II} are largely unknown. It is conceivable, however, that such demand is linked to the high firing frequency of brainstem neurons that are in constant dynamic activity compared to other brain regions in which repetitive firing activity may not be essential. Presumably, altered neuronal function within the brainstem consequent to NaChα_{II} deficiency may affect the integrated responses of the respiratory and/or cardiovascular control systems and, in turn, promote hypoxia, oxidative stress, and cell demise.

It is arguable that the NaChα_{II} deficit triggers a developmental compensation with a consequent up-regulation of other genes that mediate a toxic gain of function. This view is inconsistent with evidence that NaCh blockade exerts a neuroprotective action against hypoxia-induced neuronal death (e.g., Probert et al., 1997), information that forms a basis for considering NaCh blockers appropriate leads to be developed into neuroprotective agents for acute and chronic CNS injury (Obrenovitch, 1997).

While the activity of voltage-gated sodium channels underlies the rising phase of the action potential, voltage-gated potassium channels are responsible for its descent (Armstrong and Hille, 1998). Two K^+ channel genes have been deleted, and null mice were generated. $K_V 1.1^{-/-}$ mice exhibit epilepsy (Smart et al., 1998), whereas $K_V 4.1^{-/-}$ mice display motor skill impairments and reduced body weight but no epileptic seizures (Ho et al., 1997). Both types of mutant mice reach adulthood and show no apparent

autonomic dysfunction or signs of increased neuronal death (Smart et al., 1998; Ho et al., 1997). In contrast, the NaChα$_{II}$ appears to be critical to sustaining homeostatic processes reactive to oxygen starvation and may be involved in preventing the ensuing cell death cascade. The fact that expression of other NaChα subtypes appears to be insufficient to compensate for the NaChα$_{II}$ deficiency suggests a tightly regulated neuron-specific control of NaChα$_{II}$ expression.

The NaChα$_{II}$ knockout mouse provides an animal system for investigating the role of this channel (or, more precisely, the effect of its absence) on the neural control of breathing and probing its involvement in the cellular mechanisms for the prevention of cell destruction as triggered by extracellular signals such as oxygen deprivation. In this context, information from such studies may provide valuable insights into the role of neuronal apoptosis in respiratory disorders such as sudden infant death syndrome (cf. Waters et al., 1999). It will be interesting to determine whether the selective overexpression of the antiapoptotic protein Bcl-2 in neurons (Martinou et al., 1994; Bogdanov et al., 1999) would prevent the activation of the cell death cascade or attenuate the oxidative stress-induced cell death (Shimizu et al., 1995; Bogdanov et al., 1999) and thereby lead to the rescue of the NaChα$_{II}^{-/-}$ mice. These possibilities are currently being tested, using mice overexpressing Bcl-2 (Martinou et al., 1994).

REFERENCES

Ahmed, C. M., D. H. Ware, S. C. Lee, C. D. Patten, A. V. Ferrer-Montiel, A. F. Schinder, J. D. McPherson, C. B. Wagner-McPherson, J. J. Wasmuth, G. A. Evans, and M. Montal. 1992. Primary structure, chromosomal localization, and functional expression of a voltage-gated sodium channel from human brain. *Proc. Natl. Acad. Sci. USA.* 89: 8220–8224.

Armstrong, C. M., and B. Hille. 1998. Voltage-gated ion channels and electrical excitability. *Neuron.* 20:371–380.

Banasiak, K. J., and G. G. Haddad. 1998. Hypoxia-induced apoptosis: effect of hypoxic severity and role of *p53* in neuronal cell death. *Brain Res.* 797:295–304.

Beckh, S., M. Noda, H. Lubbert, and S. Numa. 1989. Differential regulation of three sodium channel messenger RNAs in the rat central nervous system during development. *EMBO J.* 8:3611–3616.

Ben-Sasson, S. A., Y. Sherman, and Y. Gavrieli. 1995. Identification of dying cells—in situ staining. *Methods Cell Biol.* 46:29–39.

Bogdanov, M. B., R. J. Ferrante, G. Mueller, L. E. Ramos, J. C. Martinou, and M. F. Beal. 1999. Oxidative stress is attenuated in mice overexpressing BCL-2. *Neurosci. Lett.* 262:33–36.

Capecchi, M. R. 1989. Altering the genome by homologous recombination. *Science.* 244:1288–1292.

Catalano, S. M., and C. J. Shatz. 1998. Activity-dependent cortical target selection by thalamic axons. *Science.* 281:559–562.

Catterall, W. A. 1995. Structure and function of voltage-gated ion channels. *Annu. Rev. Biochem.* 64:493–531.

Couraud, F., N. Martin-Moutot, A. Koulakoff, and Y. Berwald-Netter. 1986. Neurotoxin-sensitive sodium channels in neurons developing in vivo and in vitro. *J. Neurosci.* 6:192–198.

Felts, P. A., S. Yokoyama, S. Dib-Hajj, J. A. Black, and S. G. Waxman. 1997. Sodium channel alpha-subunit mRNAs I, II, III, NaG, Na6 and hNE (PN1), different expression patterns in developing rat nervous system. *Mol. Brain Res.* 45:71–82.

Garcia, K. D., L. K. Sprunger, M. H. Meisler, and K. G. Beam. 1998. The sodium channel Scn8a is the major contributor to the postnatal developmental increase of sodium current density in spinal motoneurons. *J. Neurosci.* 18:5234–5239.

Gray, P. A., J. C. Reckling, C. M. Bocchiaro, and J. L. Feldman. 1999. Modulation of respiratory frequency by peptidergic input to rhytmogenic neurons in the pre-Bötzinger complex. *Science.* 286:1566–1568.

Hamill, O. P., A. Marty, E. Neher, B. Sakmann, and F. J. Sigworth. 1981. Improved patch-clamp techniques for high-resolution current recording from cells and cell-free membrane patches. *Pflügers Arch. Eur. J. Physiol.* 391:85–100.

Hartshorne, R. P., B. U. Keller, J. A. Talvenheimo, W. A. Catterall, and M. Montal. 1985. Functional reconstitution of the purified brain sodium channel in planar lipid bilayers. *Proc. Natl. Acad. Sci. USA.* 82: 240–244.

Ho, C. S., R. Grange, and R. H. Joho. 1997. Pleiotropic effects of a disrupted K$^+$ channel gene, reduced body weight, impaired motor skill and muscle contraction, but no seizures. *Proc. Natl. Acad. Sci. USA.* 94:1533–1538.

Ikonomidou, C., F. Bosch, M. Miksa, P. Bittigau, J. Vöckler, K. Dikranian, T. Tenkova, V. Stefovska, L. Turski, and J. W. Olney. 1999. Blockade of NMDA receptors and apoptotic neurodegeneration in the developing brain. *Science.* 283:70–74.

Isom, L. L., T. Scheuer, A. B. Brownstein, D. S. Ragsdale, B. J. Murphy, and W. A. Catterall. 1995. Functional co-expression of the β1 and type IIA α subunits of sodium channels in a mammalian cell line. *J. Biol. Chem.* 270:3306–3312.

Katz, L. C., and C. J. Shatz. 1996. Synaptic activity and the construction of cortical circuits. *Science.* 274:1133–1138.

Ma, J. Y., W. A. Catterall, and T. Scheuer. 1997. Persistent sodium currents through brain sodium channels induced by G protein βγ subunits. *Neuron.* 19:443–452.

Martinou, J. C., M. Dubois-Dauphin, J. K. Staple, I. Rodriguez, H. Frankowski, M. Missotten, P. Albertini, D. Talabot, S. Catsicas, C. Pietra, and J. Huarte. 1994. Overexpression of BCL-2 in transgenic mice protects neurons from naturally occurring cell death and experimental ischemia. *Neuron.* 13:1017–1030.

McCormick, K. A., J. Srinivasan, K. White, T. Scheuer, and W. A. Catterall. 1999. The extracellular domain of the β1 subunit is both necessary and sufficient for β1-like modulation of sodium channel gating. *J. Biol. Chem.* 274:32638–32646.

Masliah, E., M. Mallory, M. Alford, S. Tanaka, and L. A. Hansen. 1998a. Caspase dependent DNA fragmentation might be associated with excitotoxicity in Alzheimer disease. *J. Neuropathol. Exp. Neurol.* 57: 1041–1052.

Masliah, E., J. Raber, M. Alford, M. Mallory, M. P. Mattson, D. Yang, D. Wong, and L. Mucke. 1998b. Amyloid protein precursor stimulates excitatory amino acid transport. Implications for roles in neuroprotection and pathogenesis. *J. Biol. Chem.* 273:12548–12554.

Masliah, E., A. Sisk, M. Mallory, L. Mucke, D. Schenk, and D. Games. 1996. Comparison of neurodegenerative pathology in transgenic mice overexpressing V717F beta-amyloid precursor protein and Alzheimer's disease. *J. Neurosci.* 16:5795–5811.

Noda, M., T. Ikeda, H. Suzuki, H. Takeshima, T. Takahashi, M. Kuno, and S. Numa. 1986. Expression of functional sodium channels from cloned cDNA. *Nature.* 322:826–828.

Obrenovitch, T. P. 1997. Sodium and potassium channel modulators: their role in neuroprotection. *Int. Rev. Neurobiol.* 40:109–135.

Onimaru, H., and I. Homma. 1992. Whole cell recordings from respiratory neurons in the medulla of brainstem-spinal cord preparations isolated from newborn rats. *Pflügers Arch.* 420:399–406.

Patton, D. E., L. L. Isom, W. A. Catterall, and A. L. Goldin. 1994. The adult brain $\beta1$ subunit modifies activation and inactivation gating of multiple sodium channel α subunits. *J. Biol. Chem.* 269:17649–17655.

Planells-Cases, R., M. Caprini, E. M. Rockenstein, E. Masliah, C. Murre, and M. Montal. 1999. A voltage-gated sodium channel knockout mouse. *Biophys. J.* 76:A79.

Plummer, N. W., and M. H. Meissler. 1999. Evolution and diversity of mammalian sodium channel genes. *Genomics.* 57:3233–3331.

Portera-Cailliau, C., D. L. Price, and L. J. Martin. 1997. Excitotoxic neuronal death in the immature brain is an apoptosis-necrosis morphological continuum. *J. Comp. Neurol.* 378:70–87.

Probert, A. W., S. Borosky, F. W. Marcoux, and C. P. Taylor. 1997. Sodium channel modulators prevent oxygen and glucose deprivation injury and glutamate release in rat neocortical cultures. *Neuropharmacology.* 36:1031–1038.

Raman, I. M., L. K. Sprunger, M. H. Meisler, and B. P. Bean. 1997. Altered subthreshold sodium currents and disrupted firing patterns in Purkinje neurons of Scn8a mutant mice. *Neuron.* 19:881–891.

Reckling, J. C., J. Champagnat, and M. Denavit-Saubie. 1996. Electroresponsive properties and membrane potential trajectories of three types of inspiratory neurons in the newborn mouse brainstem in vitro. *J. Neurophysiol.* 75:795–810.

Reckling, J. C., and J. L. Feldman. 1998. Pre-Bötzinger complex and pacemaker neurons: hypothesized site and kernel for respiratory rhythm generation. *Annu. Rev. Physiol.* 60:385–405.

Rockenstein, E. M., L. McConlogue, H. Tan, M. Power, E. Masliah, and L. Mucke. 1995. Levels and alternative splicing of amyloid beta protein precursor (APP) transcripts in brains of APP transgenic mice and humans with Alzheimer's disease. *J. Biol. Chem.* 270:28257–28267.

Schaller, K. L., D. M. Krzemien, P. J. Yarowsky, B. K. Krueger, and J. H. Caldwell. 1995. A novel, abundant sodium channel expressed in neurons and glia. *J. Neurosci.* 15:3231–3242.

Shimizu, S., Y. Eguchi, H. Kosaka, W. Kamiike, H. Matsuda, and Y. Tsujimoto. 1995. Prevention of hypoxia-induced cell death by Bcl-2 and Bcl-xL. *Nature.* 374:811–813.

Smart, S. L., V. Lopantsev, C. L. Zhang, C. A. Robbins, H. Wang, S. Y. Chiu, P. A. Schwartzkroin, A. Messing, and B. L. Tempel. 1998. Deletion of the $K_V1.1$ potassium channel causes epilepsy in mice. *Neuron.* 20:809–819.

Smith, J., K. Ballany, and D. Richter. 1992. Whole cell patch-clamp recordings from respiratory neurons in neonatal rat brainstem in vitro. *Neurosci. Lett.* 134:153–156.

Smith, M. R., R. D. Smith, N. W. Plummer, M. H. Meisler, and A. L. Goldin. 1998. Functional analysis of the mouse Scn8a sodium channel. *J. Neurosci.* 18:6093–6102.

St-John, W. M. 1998. Neurogenesis of patterns of automatic ventilatory activity. *Prog. Neurobiol.* 56:97–117.

Stuhmer, W., F. Conti, H. Suzuki, X. Wang, M. Noda, N. Yahagi, H. Kubo, and S. Numa. 1989. Structural parts involved in the activation and inactivation of the sodium channel. *Nature.* 339:597–603.

Stuhmer, W., C. Methfessel, B. Sakmann, M. Noda, and S. Numa. 1987. Patch clamp characterization of sodium channels expressed from rat brain cDNA. *Eur. Biophys. J.* 14:131–138.

Sutton, K. G., J. E. McRory, H. Guthrie, T. H. Murphy, and T. P. Snutch. 1999. P/Q-type calcium channels mediate the activity-dependent feedback of syntaxin-1A. *Nature.* 401:800–804.

Suzuki, H., S. Beckh, H. Kubo, N. Yahagi, H. Ishida, T. Kayano, M. Noda, and S. Numa. 1988. Functional expression of cloned cDNA encoding sodium channel III. *FEBS Lett.* 228:195–200.

Wallace, R. H., D. W. Wang, R. Singh, I. E. Scheffer, A. L. George, H. A. Phillips, K. Saar, A. Reis, E. W. Johnson, G. R. Sutherland, S. F. Berkovic, and J. C. Mulley. 1998. Febrile seizures and generalized epilepsy associated with a mutation in the Na^+-channel $\beta1$ subunit gene *SCN1B. Nature Genet.* 19:366–370.

Waters, K. A., B. Meehan, J. Q. Huang, R. A. Gravel, J. Michaud, and A. Cote. 1999. Neuronal apoptosis in sudden infant death syndrome. *Pediatr. Res.* 45:166–172.

Westenbroek, R. E., J. L. Noebels, and W. A. Catterall. 1992. Elevated expression of type II Na^+ channels in hypomyelinated axons of shiverer mouse brain. *J. Neurosci.* 12:2259–2267.

Xia, Y., and G. G. Haddad. 1994. Postnatal development of voltage-sensitive Na^+ channels in rat brain. *J. Comp. Neurol.* 345:279–287.

Yang, N., S. Ji, M. Zhou, L. J. Ptacek, R. L. Barchi, R. Horn, and A. L. George, Jr. 1994. Sodium channel mutations in paramyotonia congenita exhibit similar biophysical phenotypes in vitro. *Proc. Natl. Acad. Sci. USA.* 91:12785–12789.